



Minerva Access is the Institutional Repository of The University of Melbourne

Author/s:

Taha, M;Walia, S;Ahmed, T;Headland, D;Withayachumnankul, W;Sriram, S;Bhaskaran, M

Title:

Insulator-metal transition in substrate-independent VO₂ thin film for phase-change devices

Date:

2017-12-20

Citation:

Taha, M., Walia, S., Ahmed, T., Headland, D., Withayachumnankul, W., Sriram, S. & Bhaskaran, M. (2017). Insulator-metal transition in substrate-independent VO₂ thin film for phase-change devices. *Scientific Reports*, 7 (1), <https://doi.org/10.1038/s41598-017-17937-3>.

Persistent Link:

<https://hdl.handle.net/11343/347221>

License:

[CC BY](#)

OPEN

Insulator–metal transition in substrate-independent VO₂ thin film for phase-change devices

Mohammad Taha¹, Sumeet Walia¹, Taimur Ahmed¹, Daniel Headland², Withawat Withayachumnankul², Sharath Sriram¹ & Madhu Bhaskaran¹

Vanadium has 11 oxide phases, with the binary VO₂ presenting stimuli-dependent phase transitions that manifest as switchable electronic and optical features. An elevated temperature induces an insulator-to-metal transition (IMT) as the crystal reorients from a monoclinic state (insulator) to a tetragonal arrangement (metallic). This transition is accompanied by a simultaneous change in optical properties making VO₂ a versatile optoelectronic material. However, its deployment in scalable devices suffers because of the requirement of specialised substrates to retain the functionality of the material. Sensitivity to oxygen concentration and larger-scale VO₂ synthesis have also been standing issues in VO₂ fabrication. Here, we address these major challenges in harnessing the functionality in VO₂ by demonstrating an approach that enables crystalline, switchable VO₂ on any substrate. Glass, silicon, and quartz are used as model platforms to show the effectiveness of the process. Temperature-dependent electrical and optical characterisation is used demonstrating three to four orders of magnitude in resistive switching, >60% chromic discrimination at infrared wavelengths, and terahertz property extraction. This capability will significantly broaden the horizon of applications that have been envisioned but remained unrealised due to the lack of ability to realise VO₂ on any substrate, thereby exploiting its untapped potential.

Vanadium dioxide (VO₂) presents a characteristic temperature-dependent insulator-to-metal transition (IMT). While other materials (including other oxides of vanadium) demonstrate IMT, VO₂ is significant for switching near an electronics-compatible temperature of ~68 °C^{1–6}. This change in electrical properties is accompanied by a simultaneous transition in optical properties, wherein the material changes from being transparent to nearly opaque at infrared (IR) wavelengths. As a result, the temperature-dependent transition in electrical and optical properties of VO₂ can be exploited for a range of applications such as smart windows^{7–9}, electro-optic modulators¹⁰, memory devices¹¹, terahertz systems^{12,13}, thermal actuators¹⁴, Mott transistors¹⁵, strain sensors¹⁶, and thermo/electrochromic layers¹⁷. Significantly, the ability to synthesis high quality VO₂ films has greater consequences as doping with W or Mo can lower the IMT temperature closer to ambient conditions^{18–20}.

While the relationship between the stoichiometry, microstructure, and the nature and degree of the IMT is still a topic of research, the interplay between the concentration of vanadium ions in the multiphase VO₂^{21–23}, and the role of film thickness, grain size distribution, and crystallinity makes the fabrication highly process-dependent and substrate-dependent^{24–26}. Traditionally, deposition techniques used for VO₂ growth are heavily impacted by oxygen concentration in the growth chamber making repeatability and tunability difficult. Furthermore, large-scale deposition of VO₂ thin films has been a perennial hurdle for industrial applications. Well-known techniques such as pulsed-laser deposition (PLD) are used to grow crystalline VO₂; however, PLD cannot cover large surface areas making deposition of thin VO₂ thin films on large-scale substrates unattainable. PLD technique maintains critical drawbacks of limited deposition uniformity and lack of cluster-free deposition. Although it can be implemented on a variety of substrates such as glass, sapphire and silicon, scaling up is still an obstacle²⁷. There are a few reports that study the optimisation of the quality of VO₂ thin films deposited using the sputtering process^{13,28,29}. However, these reports suggest that single crystal substrates such as sapphire are a key requirement for realising high quality VO₂ thin films, with the desired electrical and optical properties. Other reports utilise

¹Functional Materials and Microsystems Research Group and Micro Nano Research Facility, RMIT University, Melbourne, Victoria, 3001, Australia. ²School of Electrical and Electronic Engineering, The University of Adelaide, South Australia, 5005, Australia. Correspondence and requests for materials should be addressed to M.T. (email: mohammad.taha@unimelb.edu.au) or M.B. (email: madhu.bhaskaran@rmit.edu.au)

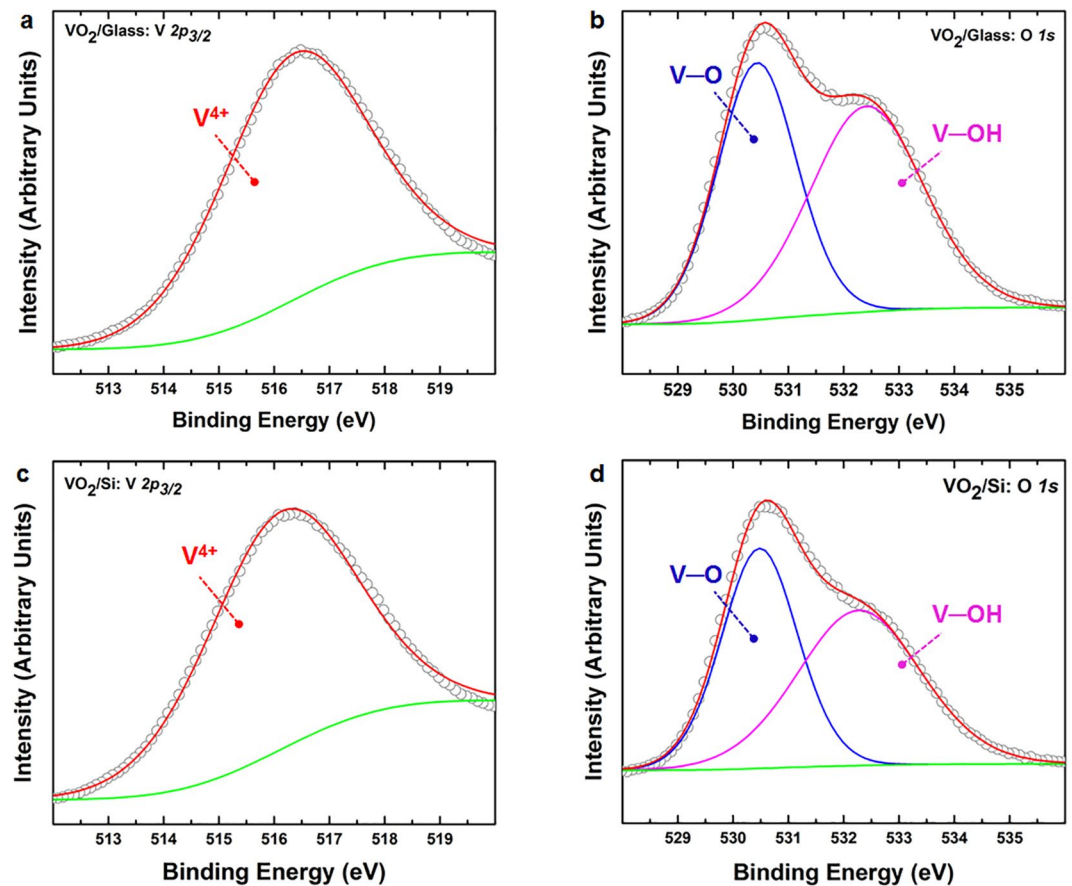


Figure 1. Core-level XPS spectra of vanadium ($V 2p_{3/2}$) in (a) and (c) and oxygen ($O 1s$) in (b) and (d) collected from post-deposition annealed thin films sputter-deposited on glass and silicon substrates.

sputtering and successfully show VO_2 thin films on glass and silicon^{30,31}. However, substrate-independence and a simultaneous complete characterisation of electrical and optical properties of the same set of thin films is still lacking. As a result, the limitation of substrate choice has restricted applications using VO_2 despite its unique and versatile characteristics.

This work presents a thin film deposition process by magnetron sputtering to high quality VO_2 thin films. The process is substrate-independent and highly repeatable. Depositions on three different substrates – glass, quartz, and float-zone silicon (with a resistivity $> 50 \Omega.m$) – are carried out to show the flexibility of the process. An IMT where the resistivity reversibly changes by up to four orders of magnitude (typically three orders of magnitude) is observed for VO_2 thin films on all three substrates. This is also accompanied by a reversible change in transmission characteristics in the infrared region of the optical spectrum, with $>60\%$ discrimination. A systematic analysis of the effects of film thickness and the sputtering gas ratios on the performance of the VO_2 films is also presented.

Results

VO_2 thin films morphology and composition analysis. To assess the chemical composition of the vanadium oxide thin films and establish presence of the VO_2 phase, X-ray photoelectron spectroscopic (XPS) analyses are carried out on as-grown and post-annealed thin films. Figure 1 shows high resolution XPS spectra of $V 2p_{3/2}$ and $O 1s$ collected from the post-deposition annealed thin film. The $V 2p_{3/2}$ spectrum in Fig. 1a shows a single peak centered at 516.4 eV which corresponds to the V^{4+} oxidation state^{32–34}. The $O 1s$ spectrum in Fig. 1b can be fitted with two components with peak positions at 530.4 eV and 532.4 eV attributed to V–O and V–OH, respectively³⁵. The combination of the V and O oxidation states confirms the presence of the VO_2 phase exclusively, given only the V^{4+} oxidation state is observed. Figure 1c and d show similar $V 2p_{3/2}$ and $O 1s$ peaks for post deposition annealed samples on Si substrates illustrating the substrate independent stoichiometry obtained using our proposed recipe.

The composition of the post-deposition annealed thin film does not show any difference in the oxidation state of vanadium (*i.e.*, V^{4+}) as compared to the as-grown film (See Supplementary information, Figure S1). This indicates that post-deposition annealing only changes the crystallinity of the films without affecting the chemical composition of the sputtered oxide. This was further verified using X-ray diffraction (XRD) studies.

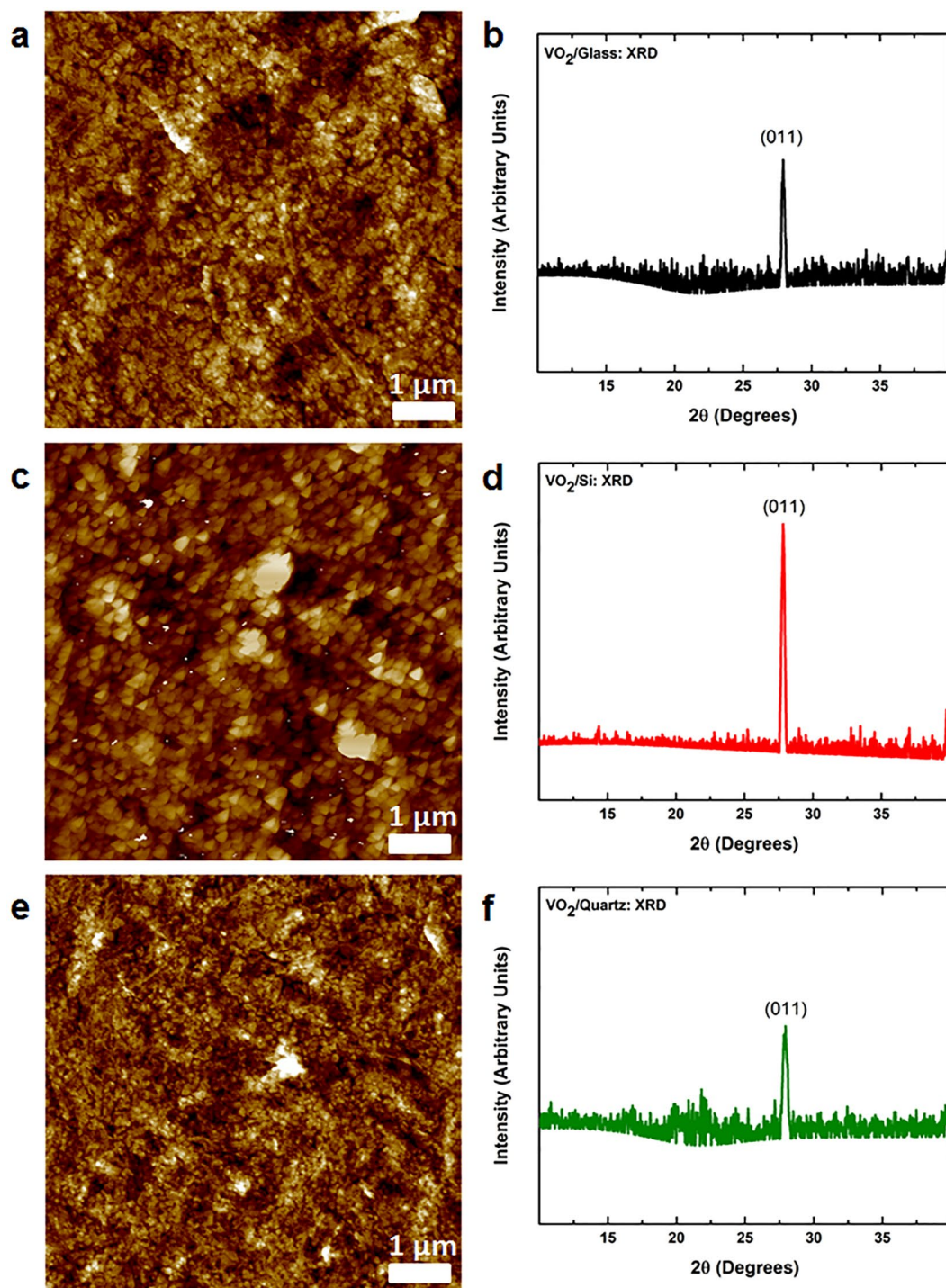


Figure 2. Characterisation of VO₂ thin films: Atomic force micrographs for post-deposition annealed VO₂ thin films on (a) glass (c) high resistivity silicon and (e) quartz; X-ray diffractograms for films deposited on (b) glass (d) high resistivity silicon and (f).

To substantiate a valid comparison between films deposited on different substrates, we do not rely only on composition. Here, we investigate surface morphology and crystallinity using atomic force microscope (AFM) topography scans and X-ray diffraction (XRD) studies.

Figures 2a,c,e show AFM topography scans of post-deposition annealed VO₂ thin films for glass, silicon and quartz, respectively. Scans of post-deposition annealed VO₂ thin films show well-defined grains. The average surface roughness of the films is calculated to be 3.64, 3.39 and 3.86 nm on glass, silicon and quartz respectively. We further investigate our X-ray diffractograms of post-deposition annealed VO₂ thin films on glass, silicon and quartz substrates. Figure 2b,d and f show X-ray diffractograms for crystalline films on all three substrates. While the room temperature deposited films are amorphous or nanocrystalline with no long-range lattice arrangement

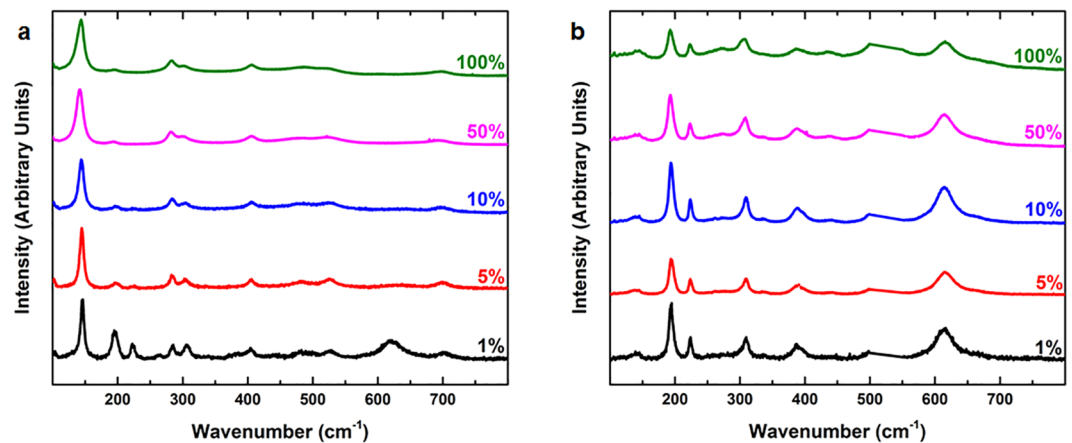


Figure 3. Raman spectrum of the post-deposition annealed VO₂ thin film fabricated on (a) glass and (b) silicon acquired with different laser intensities. Percentages correspond to incident power intensities of 532 nm laser, where 100% is 9 mW.

Raman Peak	Phonon mode	Reference	Raman Peak	Phonon mode	Reference
140	—	39,40,43–45	395	A _g	39,40,43–45
195	A _g	39,40,43–45	439	B _g	39,40,43–45
225	A _g	39,40,43–45	489	B _g	39,40,43–45
264	B _g	39,40,43–45	503	A _g	39,40,43–45
280	—	16,42,44	525	A _g	38,41
304	A _g	39,40,43–45	585	B _g	39,40,43–45
337	B _g	39,40,43–45	615	A _g	39,40,43–45
385	A _g	39,40,43–45	700	—	41,44

Table 1. Raman vibrational modes for the VO₂ thin films.

observed, the post-deposition annealed films on glass, silicon and quartz show a preferred (011) alignment at a θ of $\sim 27.9^\circ$, which is characteristic of stoichiometric VO₂^{1,36}. Literature reports indicate that the most effective transition switching in VO₂ occurs across the (011) and (0 $\bar{1}$ 1) directions of the monoclinic structure³⁷. To gain further insight, full width at half maximum (FWHM) was calculated from the XRD spectra. A FWHM of 0.3, 0.3 and 0.4 for glass, silicon and quartz is obtained. It is known that the FWHM is heavily influenced by discrepancies in crystal structures, however, this is not the case for the films reported in this study as FWHM shows little change for the films deposited on different substrates (See Supplementary information, Figure S2 for FWHM calculations).

Even though as-grown films possess the same composition as post-deposition annealed films they do not display IMT or thermochromism in the infrared region of the optical spectra (See Supplementary information, Figure S3).

Figure 3 shows the Raman spectra of the post-deposition annealed films fabricated on glass and Si. Peaks and their associated phonon vibrations are summarised in Table 1. These can be assigned to the A_g and B_g phonon vibration modes of VO₂, which is consistent with reports in literature^{1,16,38–45}. It should be noted that the 195 and 615 cm⁻¹ features that signify the V–O bond vibrations are relatively weak in intensity. We attribute this to the highly localised laser induced heating during the Raman measurements which could induce a phase change of VO₂ at the measurement location. This phase change is known to significantly reduce the intensity of these vibration modes³⁶. Figure 3a,b show the evolution of the Raman spectra with varying incident laser powers. Although Raman results show evidence that the films are indeed VO₂ since the peaks are consistent with literature (Table 1), the films are affected by localised heating. This effect is discussed in more detail in the discussion section, but since Raman spectroscopy changes the observation of phonon vibrations making absolute conclusion about the full characteristics of VO₂ thin films on those substrates using only Raman spectroscopy is unreliable. Therefore, we utilise a combination of XPS, AFM and the XRD analysis of the thin films alongside the Raman spectra to form a clearer idea of the nature of VO₂ films synthesised using our method. AFM topography scans show well-defined grains and an average surface roughness that is consistent on glass, silicon and quartz. XRD crystallinity matching and FWHM indicate similar crystallinity between the VO₂ films deposited on different substrates reported in this work. The abovementioned compositional, phase and crystallinity characterisations clearly show that the films deposited through the reported recipe are VO₂ thin films without the presence of any additional phase.

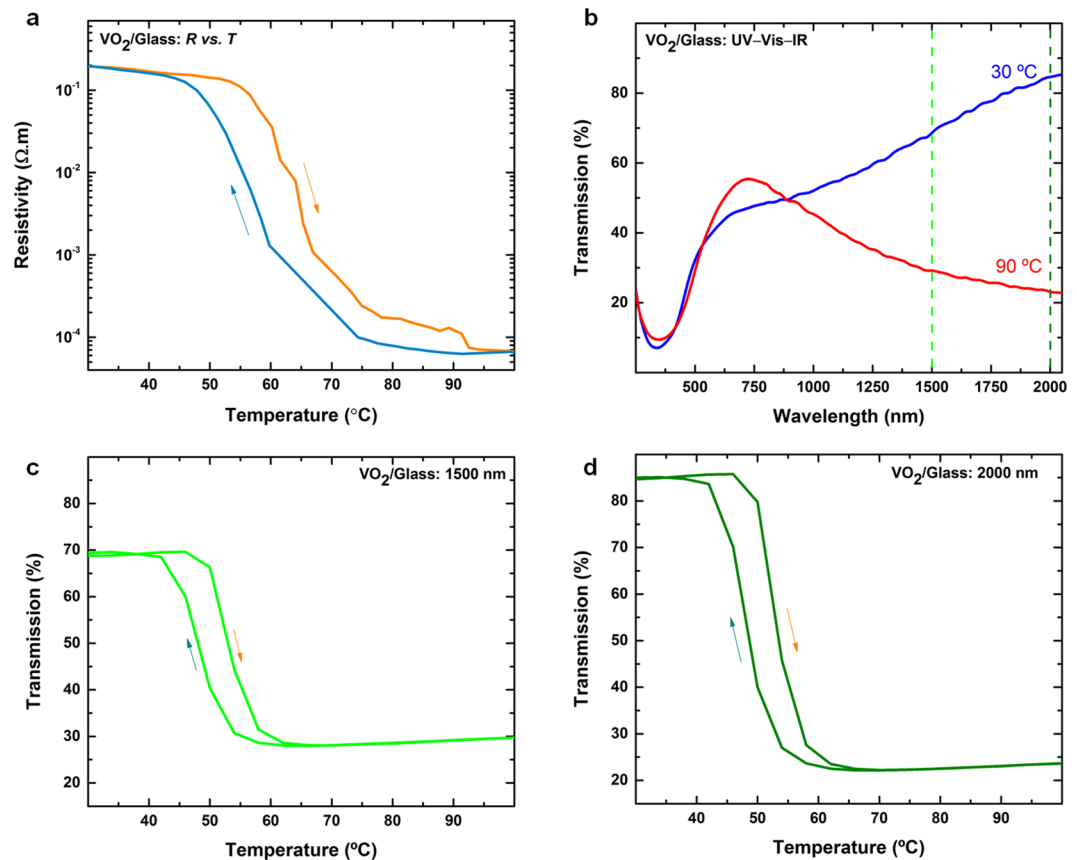


Figure 4. (a) Resistivity vs. temperature for a VO₂ thin film on glass. (b) Corresponding UV-Vis-IR optical transmission. Optical transmission vs. temperature for the VO₂ thin films on glass acquired at optical wavelengths of (c) 1500 nm and (d) 2000 nm.

Oxygen partial pressure (%)	Deposition duration (min)	Film thickness (nm)	Switching ratio R_{30}/R_{90}	Rate of change ($\Omega.m/^{\circ}C$)	Rate of change ($\Omega.m/min$)	Optical switching at 2000 nm (%)
30	15	50.4	1,289	8	32	~40%
30	30	100.8	455	38	150	~58%
30	45	151.2	2,309	28	111	~60%
50	15	31.5	251	15	60	~25%
50	30	63.0	714	7	30	~50%
50	45	94.5	1,433	21	84	~63%

Table 2. Summary of deposition conditions and the corresponding IMT switching performance.

Insulator-to-metal transition (IMT), electrical and optical characterization. We now characterise the electrical resistivity of the VO₂ thin films using the four-point probe technique. The temperature-dependent resistivity of the VO₂ thin films on glass (deposited at 30% Ar:O₂ ratio for 45 min) is shown in Fig. 4a and shows a drop in resistivity of four orders of magnitude at a temperature of ~69°C. The amplitude of the IMT is obtained from the resistivity ratio (R_{90}/R_{30}) at temperatures of 90°C and 30°C, respectively. An obvious thermal hysteresis is also observed between the heating and cooling cycles. Table 2 summarizes the electrical and switching performance for VO₂ thin films with respect to varying oxygen concentrations and deposition duration. It is seen that the films sputtered at 30% O₂ for 45 min show the highest magnitude of IMT resistive switching (explaining choice of films for detailed characterisation) indicating a key role played by the oxygen concentration during deposition and the thickness of the film.

Figure 4b shows a comparison of the optical transmission of a VO₂ thin film at 30°C and 90°C across the ultra-violet, visible, and infrared spectrum (UV-Vis-IR spectroscopy). While the change in the visible range is not significant, the discrimination between the ‘insulator’ (transparent) and ‘metal’ (opaque) states for higher wavelengths is apparent. This agrees with known thermochromic NIR characteristics of VO₂^{4,6,8,9,12,13,18,22,29}. IMT is reversible and repeatable as films display recovery after the removal of the thermal trigger for the IMT. Films undergo consistent and repeatable IMT when heat is re-applied (See Supplementary information, Figure S4).

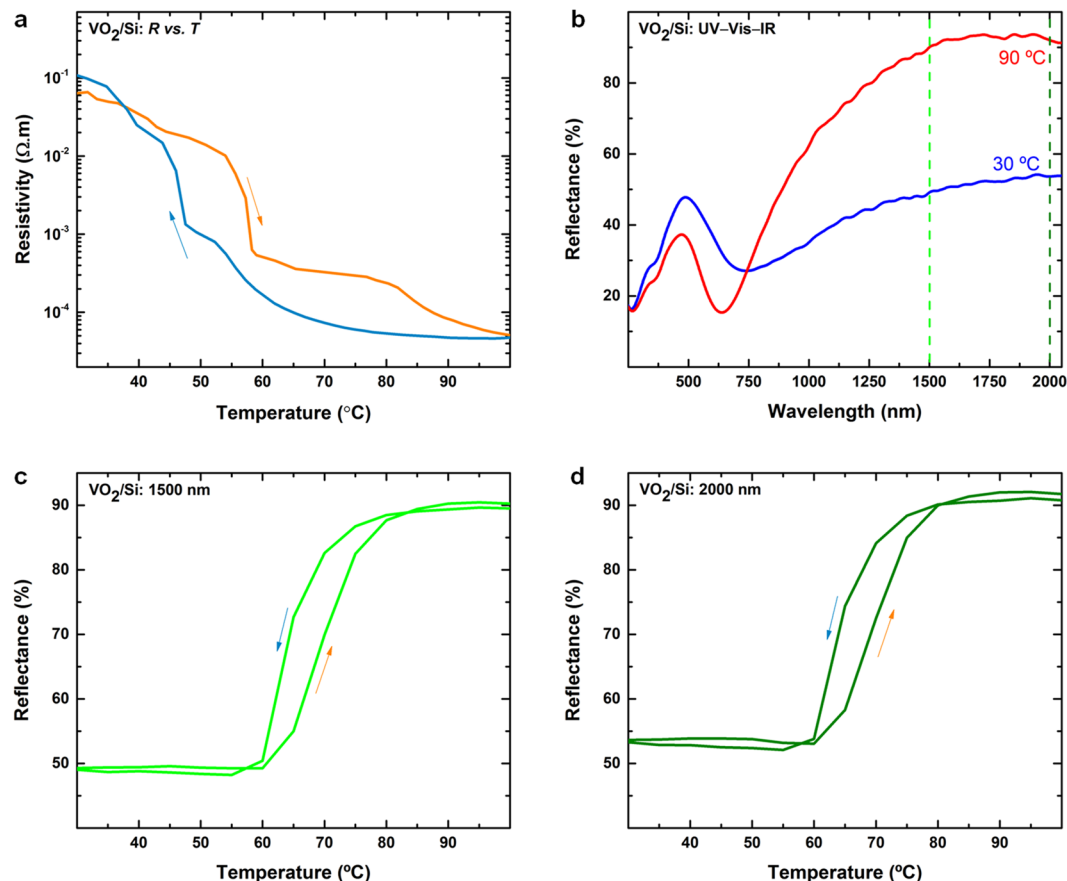


Figure 5. (a) Resistivity vs. temperature for a VO₂ thin film on silicon. (b) Corresponding UV-Vis-IR reflectance performance. Optical reflectance vs. temperature for a VO₂ thin films on silicon acquired at optical wavelengths of (c) 1500 nm and (d) 2000 nm.

To further substantiate this observation, temperature-dependent (both heating and cooling cycles) transmission spectra are obtained at two infrared wavelengths of 1500 and 2000 nm and are shown in Fig. 4c,d, respectively. An obvious and significant change in the infrared transmittance can be observed throughout the temperature band where the IMT occurs. From a transmittance of ~70% at 30 °C (insulating phase), the value drops to below 28% and 25% at 90 °C (metallic phase) for 1500 and 2000 nm, respectively. This further elucidates that the optical switching ratios in VO₂ become larger as we move to longer wavelengths. The optical switching ratios for the various samples fabricated in this study are listed in Table 2. We also note that the transition temperatures for the electrical and the optical measurements are slightly different, which we attribute to discrepancies and collection times between the electrical and optical measurement systems.

According to the Beer-Lambert law, the optical transmittance is exponentially dependent on the film thickness. The data listed in Table 2 confirms that the thickest VO₂ film exhibits the best electrical and optical switching properties. However, there will be an optimal limit, beyond which the considerable number of charge carriers in the system will inhibit switching owing to scattering at point defects in the crystal lattice. It can be therefore concluded that the infrared switching properties of the VO₂ thin films depend on thickness as well as the stoichiometry. Additionally, an informed choice of sputtering power needs to be made to obtain a delicate balance between the formation of secondary phases that occurs if the power is too low and poisoning of the high-purity vanadium target if the power is too high. A comparison of electrical and optical properties for the as-grown and annealed VO₂ films (See Supplementary information, Figure S3) reaffirms that annealing-induced crystallinity and the formation of coalesced grain structure as observed in AFM scans are important for desirable electrical and optical transitions. Post-deposition annealing in our work makes the films crystalline which is important to achieve the characteristic IMT. Such a transition cannot occur on as-deposited amorphous films due to a lack of carriers.

Substrate-independent VO₂ thin films. The ability to synthesise such high-performance films on amorphous glass substrates is a significant outcome. To demonstrate that this synthesis approach is substrate-independent, we perform depositions on silicon and quartz substrates. Electrical and optical characteristics of a VO₂ thin film deposited on a silicon substrate are shown in Fig. 5. Figure 5a,b shows that the IMT and the optical transition of the thin films are maintained on a silicon substrate. It should be noted that the different electrical properties of silicon affect quality of four-point probe measurements, while reflectivity is measured in place of transmission for UV-Vis-IR spectroscopy. Further variations in the electrical behaviour can also arise

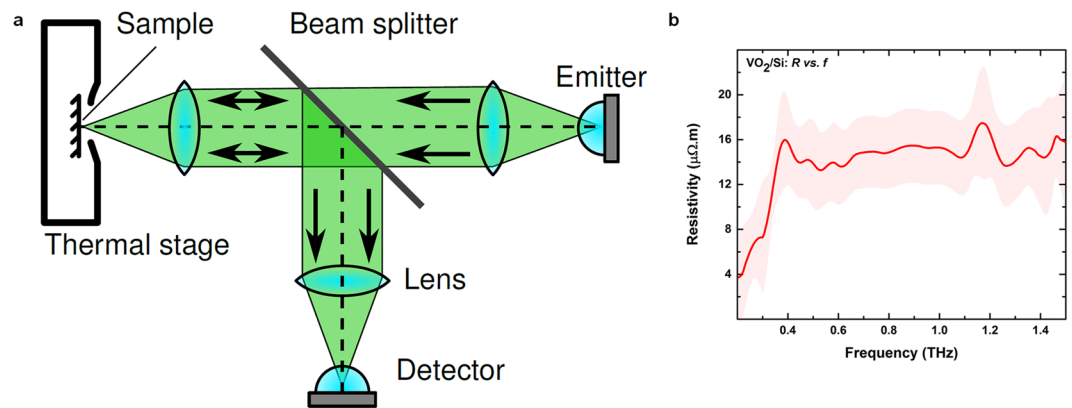


Figure 6. (a) Reflective terahertz time-domain spectroscopy setup, where the sample is heated using a thermal stage. (b) Extracted resistivity of metallic-phase VO₂ on Si in the terahertz range, with error bars at one standard deviation shown as a transparent region.

from the difference in the thermal properties and the thickness of the substrates. To assess the reflectance at different infrared wavelengths, cyclic reflection data is collected at two infrared wavelengths of 1500 and 2000 nm (as in the case of VO₂ on glass) and are shown in Fig. 5c,d, respectively. From a reflectance of ~49% (1500 nm) and ~52% (2000 nm) at 30 °C (electrically insulating phase), the value rises to around 90% (1500 nm) and 91% (2000 nm) at 90 °C (metallic phase). It is seen that the electrical IMT switching is at least three orders of magnitude and optical transition is at least 40% irrespective of the substrate.

Similar deposition and characterisation was undertaken with success on quartz substrates to achieve electrical change of 10^4 and optical discrimination of 55% at 2000 nm (See Supplementary information, Figure S5). Room temperature deposition results in VO₂ with the correct chemical composition. The major factor affecting the functionality of the metal oxide is the crystallinity and number of oxygen vacancies. It is seen that the transition temperatures for all the substrates lie in a range that is in line with the expectation from the VO₂ phase^{1–6}.

It is well-known that the properties of metals are frequency-dependent⁴⁶. Hence, in order to assess the high-frequency resistivity of the VO₂ thin films synthesised on this study, we perform characterisation at terahertz-range frequencies. Figure 6a shows the terahertz time-domain spectroscopy (THz-TDS) setup used. THz-TDS is an effective technique for extracting carrier concentration and conductive properties of thin films. The VO₂ thin films on silicon was characterised at high temperature (metallic state). The results are shown in Fig. 6b with resistivity of $\sim 0.5 \times 10^{-4} \Omega \cdot \text{m}$ across a frequency range of 0.5–2.5 THz (See Supplementary information, S6 for details of resistivity extraction). This is consistent with the DC resistivity results presented in Figs 4a and 5a. This highlights that VO₂ retains its key electronic features even at high frequencies, and therefore, is a promising material for applications in the terahertz domain.

Discussion

We have developed a substrate-independent recipe to deposit crystalline VO₂ thin films. Using room temperature deposition and low-vacuum post-annealing at 550 °C produces VO₂ thin films on glass substrates with excellent electrical and optical transition. The careful balance of utilising room temperature deposition to control stoichiometry and post-deposition annealing to define crystalline phase results in single-phase, preferentially-oriented VO₂ films. The characteristic IMT is verified both electrically and optically with a dramatic change observed in transmission at infrared wavelengths. The versatility of the process is verified by depositing and characterising VO₂ films on silicon and quartz.

We observe that the thermal conductivity of the substrate plays a crucial role in characterisations measurements. This is evident from the Raman spectra obtained on glass and silicon at different laser powers. The highly localised nature of the laser during the Raman measurements will induce a significant amount of heat which has to be dissipated through the substrate. We conducted a sequential set of measurements with varying Raman laser powers to gain more insight (Fig. 3). For the glass substrate, peaks at 195 and 615 cm⁻¹ amongst other peaks disappeared at 100% laser power. This is induced due to the build-up of heat generated due to the laser. On the other hand, the heat dissipates faster on silicon owing to its higher thermal conductivity⁴⁷ compared to glass⁴⁸, which translates to significantly smaller variations in the Raman spectra as shown in Fig. 3. Therefore, Raman spectroscopy cannot be used as a conclusive method of VO₂ films characterisation especially in the case of substrates with low thermal conductivity. Therefore, we have also used AFM, XRD and XPS to characterise the composition, topography and crystallinity of the VO₂ thin films which highlight the consistency of the recipe we propose in this study. This also highlights that the certain dissimilarities in both electrical and optical properties in VO₂ films on Si are not caused due to variations in the quality of the films but rather the thermal properties of the substrate. Alongside thermal properties and substrate thickness it is important to consider that four-point probes also measure the sheet resistance of the underlying substrate which will have an effect in the case of a semiconducting substrate like silicon. This can result in relatively lower IMT magnitudes. It must be noted that the film still maintains up to 3 orders of magnitude without an insulating layer on top of silicon which further supports the fact that the film quality is preserved regardless of the substrate. The previous conclusion is further

Target used	Vanadium (99.99%)
Distance from the target	~120 mm
Base pressure	4.0×10^{-7} Torr
Sputtering pressure	2.8×10^{-3} Torr
Ar:O ₂ flow rate	12.25:5.25 sccm (for 30%)
Sputtering power	200 W
Pulse frequency, reverse time	25 kHz, 5 μ s
Substrate temperature	Ambient

Table 3. Sputtering parameters for depositing VO₂ thin films using pulsed DC magnetron sputtering.

verified in the case of the quartz substrate, where the characteristics are not different. Since glass and quartz have similar thermal conductivities, the performance of the VO₂ films fabricated on these substrates are analogous (See Supplementary Information, Figure S5). This substrate-independent method of depositing high quality VO₂ thin films can open several opportunities for creating smart windows, temperature-tunable memories, modulated nanoplasmonic surfaces, and terahertz devices.

Methods

VO₂ thin film deposition. The VO₂ thin films are deposited onto plasma-cleaned glass, silicon, and quartz substrates using the pulsed DC magnetron sputtering technique. Detailed parameters used for thin film deposition are shown in Table 3. Subsequently, the as-deposited VO₂ films are annealed in a furnace, evacuated to low vacuum to achieve a pressure of ~250 mTorr, at 550 °C for 90 min. Several deposition parameters were studied to optimise phase, composition, and switching. These are listed in Table 2, which is discussed in detail. VO₂ thin films sputtered with 30% O₂ in an Ar and O₂ gas mixture for 45 min are ~150 nm thick. All analyses and characterisation discussed in this work pertain to these films.

Spectroscopy and microanalysis. X-ray photoelectron spectroscopy (XPS) analysis is conducted using a Thermo Scientific K-Alpha instrument under ultrahigh vacuum (base pressure $< 1 \times 10^{-7}$ Pa). An aluminium K α X-ray radiation source with energy of 1486.6 eV is used. All core-level spectra of the elements are collected at pass energy of 50 eV and analysed with Advantage software. The binding energies of all principal elements are referenced to the adventitious carbon (C 1s) of binding energy 284.6 eV. Crystallography is verified using a X-ray diffraction powder analyser (D2 Phaser, Bruker). Deposited film thicknesses were measured by stylus profilometry (Dektak XT, Bruker). A Dimension Icon atomic force microscope was used to obtain surface topography. Raman spectra were obtained using a Horiba LabRAM Evolution micro-Raman system equipped with 9 mW, 532 nm laser (0.5 μ m lateral resolution, 2 s exposure) and a 50 \times objective.

Insulator-to-metal transition measurements. Electrical measurements were conducted using a Jandel cylindrical four-point probe. UV-Vis-IR transmission and reflection spectra are collected using a CRAIC 20/30 microspectrophotometer. A Linkam stage is used for heating and cooling of the sample during the electrical and optical measurements. The ramp-up and ramp-down rates are controlled at 5 °C/min while measurements are collected.

Terahertz characterisation. The terahertz-range resistivity of VO₂ is characterised using a terahertz time-domain spectroscopy (THz-TDS) setup shown in Fig. 6a. A polished high-resistivity silicon wafer is employed as a beam splitter in order to probe the response to normally-incident terahertz radiation⁴⁹, and a Linkam thermal stage is employed to heat the sample and produce the desired phase change. In order to maintain good alignment between the sample and reference measurements, self-referencing is used in this case, where the measurement of the metallic-phase sample is normalised by a corresponding measurement from the insulating-phase counterpart.

Data Availability

All relevant data is available from the authors on request.

References

- Luo, Y. Y. *et al.* Influence of sputtering power on the phase transition performance of VO₂ thin films grown by magnetron sputtering. *J. Alloys Compd.* **664**, 626–631, <https://doi.org/10.1016/j.jallcom.2015.12.222> (2016).
- Servin, R. *et al.* Unravelling the switching mechanisms in electric field induced insulator–metal transitions in VO₂ nanobeams. *J. Phys. D: Appl. Phys.* **47**, 295101 (2014).
- Guo, Y. *et al.* Evolution of structure and electrical properties with annealing time in solution-based VO₂ thin films. *J. Alloys Compd.* **622**, 913–917, <https://doi.org/10.1016/j.jallcom.2014.11.027> (2015).
- Zhang, H. *et al.* A cost-effective method to fabricate VO₂ (M) nanoparticles and films with excellent thermochromic properties. *J. Alloys Compd.* **636**, 106–112, <https://doi.org/10.1016/j.jallcom.2015.01.277> (2015).
- Nagashima, K., Yanagida, T., Tanaka, H. & Kawai, T. Influence of ambient atmosphere on metal-insulator transition of strained vanadium dioxide ultrathin films. *J. Appl. Phys.* **100**, 063714, <https://doi.org/10.1063/1.2345600> (2006).
- Wu, C., Feng, F. & Xie, Y. Design of vanadium oxide structures with controllable electrical properties for energy applications. *Chem. Soc. Rev.* **42**, 5157–5183, <https://doi.org/10.1039/C3CS35508J> (2013).
- Zhou, J. *et al.* VO₂ thermochromic smart window for energy savings and generation. *Sci. Rep.* **3**, 3029 (2013).

8. Kato, K., Song, P. K., Odaka, H. & Shigesato, Y. Study on thermochromic VO₂ films grown on ZnO-coated glass substrates for “smart windows”. *Jpn. J. Appl. Phys.* **42**, 6523 (2003).
9. Jin, P., Xu, G., Tazawa, M. & Yoshimura, K. A VO₂-based multifunctional window with highly improved luminous transmittance. *Jpn. J. Appl. Phys.* **41**, L278 (2002).
10. Markov, P. *et al.* Optically Monitored Electrical Switching in VO₂. *ACS Photonics* **2**, 1175–1182, <https://doi.org/10.1021/acsp Photonics.5b00244> (2015).
11. Lee, M. J. *et al.* Two series oxide resistors applicable to high speed and high density nonvolatile memory. *Adv. Mater.* **19**, 3919–3923 (2007).
12. Seo, M. *et al.* Active terahertz nanoantennas based on VO₂ phase transition. *Nano Lett.* **10**, 2064–2068 (2010).
13. Luo, Y. Y. *et al.* Terahertz conductivities of VO₂ thin films grown under different sputtering gas pressures. *J. Alloys Compd.* **655**, 442–447, <https://doi.org/10.1016/j.jallcom.2015.08.254> (2016).
14. Cao, J. *et al.* Colossal thermal-mechanical actuation via phase transition in single-crystal VO₂ microcantilevers. *J. Appl. Phys.* **108**, 083538 (2010).
15. Nakano, M. *et al.* Collective bulk carrier delocalization driven by electrostatic surface charge accumulation. *Nature* **487**, 459–462 (2012).
16. Hu, B. *et al.* External-Strain Induced Insulating Phase Transition in VO₂ Nanobeam and Its Application as Flexible Strain Sensor. *Adv. Mater.* **22**, 5134–5139 (2010).
17. Mlyuka, N., Niklasson, G. & Granqvist, C.-G. Mg doping of thermochromic VO₂ films enhances the optical transmittance and decreases the metal-insulator transition temperature. *Appl. Phys. Lett.* **95**, 171909 (2009).
18. Manning, T. D., Parkin, I. P., Pemble, M. E., Sheel, D. & Vernardou, D. Intelligent window coatings: atmospheric pressure chemical vapor deposition of tungsten-doped vanadium dioxide. *Chem. Mater.* **16**, 744–749 (2004).
19. Mai, L., Hu, B., Hu, T., Chen, W. & Gu, E. Electrical Property of Mo-Doped VO₂ Nanowire Array Film by Melting–Quenching Sol–Gel Method. *J. Phys. Chem. B* **110**, 19083–19086 (2006).
20. Takahashi, I., Hibino, M. & Kudo, T. Thermochromic properties of double-doped VO₂ thin films prepared by a wet coating method using polyvanadate-based sols containing W and Mo or W and Ti. *Jpn. J. Appl. Phys.* **40**, 1391 (2001).
21. Lafane, S. *et al.* Correlation of plume dynamics and oxygen pressure with VO₂ stoichiometry during pulsed laser deposition. *Appl. Phys. A* **112**, 159–164, <https://doi.org/10.1007/s00339-012-7223-9> (2013).
22. Fu, D. *et al.* Comprehensive study of the metal-insulator transition in pulsed laser deposited epitaxial VO₂ thin films. *J. Appl. Phys.* **113**, 043707, <https://doi.org/10.1063/1.4788804> (2013).
23. Narayan, J. & Bhosle, V. M. Phase transition and critical issues in structure-property correlations of vanadium oxide. *J. Appl. Phys.* **100**, 103524, <https://doi.org/10.1063/1.2384798> (2006).
24. Chen, C. *et al.* Influence of defects on structural and electrical properties of VO₂ thin films. *J. Appl. Phys.* **110**, 023707, <https://doi.org/10.1063/1.3609084> (2011).
25. Kang, L. *et al.* Effects of Annealing Parameters on Optical Properties of Thermochromic VO₂ Films Prepared in Aqueous Solution. *J. Phys. Chem. C* **114**, 1901–1911, <https://doi.org/10.1021/jp909009w> (2010).
26. Liu, H. W., Wong, L. M., Wang, S. J., Tang, S. H. & Zhang, X. H. Effect of oxygen stoichiometry on the insulator-metal phase transition in vanadium oxide thin films studied using optical pump-terahertz probe spectroscopy. *Appl. Phys. Lett.* **103**, 151908, <https://doi.org/10.1063/1.4824834> (2013).
27. Jian, J., Chen, A., Zhang, W. & Wang, H. Sharp semiconductor-to-metal transition of VO₂ thin films on glass substrates. *J. Appl. Phys.* **114**, 244301 (2013).
28. Xiong-Bang, W. *et al.* Growth mode and texture study in vanadium dioxide thin films deposited by magnetron sputtering. *J. Phys. D: Appl. Phys.* **41**, 055303 (2008).
29. Jin, P., Xu, G., Tazawa, M. & Yoshimura, K. Design, formation and characterization of a novel multifunctional window with VO₂ and TiO₂ coatings. *Appl Phys A Mater Sci Process* **77**, 455–459, <https://doi.org/10.1007/s00339-002-1460-2> (2003).
30. Sun, Y. *et al.* Anisotropic vanadium dioxide sculptured thin films with superior thermochromic properties. *Sci. Rep.* **3** (2013).
31. Xu, H. Y., Huang, Y. H., Li, J. P., Ma, F. & Xu, K. W. Effect of porous morphology on phase transition in vanadium dioxide thin films. *Journal of Vacuum Science & Technology A: Vacuum, Surfaces, and Films* **33**, 061508 (2015).
32. Silversmit, G., Depla, D., Poelman, H., Marin, G. B. & De Gryse, R. Determination of the V2p XPS binding energies for different vanadium oxidation states (V 5+ to V 0+). *J. Electron. Spectrosc. Relat. Phenom.* **135**, 167–175 (2004).
33. Koza, J. A., He, Z., Miller, A. S. & Switzer, J. A. Resistance switching in electrodeposited VO₂ thin films. *Chem. Mater.* **23**, 4105–4108 (2011).
34. Hryha, E., Rutqvist, E. & Nyborg, L. Stoichiometric vanadium oxides studied by XPS. *Surf. Interface Anal.* **44**, 1022–1025 (2012).
35. Gracia, F., Yubero, F., Espinós, J. & González-Elipe, A. First nucleation steps of vanadium oxide thin films studied by XPS inelastic peak shape analysis. *Appl. Surf. Sci.* **252**, 189–195 (2005).
36. Lopez, R. *et al.* Synthesis and characterization of size-controlled vanadium dioxide nanocrystals in a fused silica matrix. *J. Appl. Phys.* **92**, 4031–4036 (2002).
37. Booth, J. M. *et al.* Correlating the Energetics and Atomic Motions of the Metal-Insulator Transition of M1 Vanadium Dioxide. *Sci. Rep.* **6** (2016).
38. Petrov, G., Yakovlev, V. & Squier, J. Raman microscopy analysis of phase transformation mechanisms in vanadium dioxide. *Appl. Phys. Lett.* **81**, 1023–1025 (2002).
39. Kim, H.-T. *et al.* Raman study of electric-field-induced first-order metal-insulator transition in VO₂-based devices. *Appl. Phys. Lett.* **86**, 242101–242101 (2005).
40. Heckman, E. M., Gonzalez, L. P., Guha, S., Barnes, J. O. & Carpenter, A. Electrical and optical switching properties of ion implanted VO₂ thin films. *Thin Solid Films* **518**, 265–268, <https://doi.org/10.1016/j.tsf.2009.05.063> (2009).
41. Wang, X. *et al.* XRD and Raman study of vanadium oxide thin films deposited on fused silica substrates by RF magnetron sputtering. *Appl. Surf. Sci.* **177**, 8–14 (2001).
42. Okimura, K. *et al.* Temperature-dependent Raman and ultraviolet photoelectron spectroscopy studies on phase transition behavior of VO₂ films with M1 and M2 phases. *J. Appl. Phys.* **115**, 153501 (2014).
43. Pan, M. *et al.* Raman study of the phase transition in VO₂ thin films. *J. Cryst. Growth* **268**, 178–183 (2004).
44. Wu, X., Tao, Y., Dong, L., Wang, Z. & Hu, Z. Preparation of VO₂ nanowires and their electric characterization. *Mater. Res. Bull.* **40**, 315–321 (2005).
45. Ureña-Begara, F., Crunteanu, A. & Raskin, J.-P. Raman and XPS characterization of vanadium oxide thin films with temperature. *Appl. Surf. Sci.* **403**, 717–727 (2017).
46. Drude, P. Zur elektronentheorie der metalle. *Ann. Phys. (Berlin)* **306**, 566–613 (1900).
47. Shanks, H., Maycock, P., Sidles, P. & Danielson, G. Thermal conductivity of silicon from 300 to 1400 K. *Phys. Rev.* **130**, 1743 (1963).
48. Wray, K. L. & Connolly, T. J. Thermal conductivity of clear fused silica at high temperatures. *J. Appl. Phys.* **30**, 1702–1705 (1959).
49. Ung, B. S.-Y. *et al.* Dual-mode terahertz time-domain spectroscopy system. *IEEE Trans. THz Sci. Technol.* **3**, 216–220 (2013).

Acknowledgements

The authors acknowledge support from the Australian Research Council (ARC) for personnel and project support via DE160100023 (M.B.), DP170101922 (W.W., M.B.), DP130100062 (S.S.), and equipment funding through LE0882246, LE0989615, LE110100223, and LE150100001. Partial support was received through a Victoria Fellowship (M.B.) and a RMIT Foundation Malcolm Moore Award (S.W.). The authors also acknowledge the facilities and technical assistance of the Micro Nano Research Facility (MNRF) and the RMIT Microscopy and Microanalysis Research Facility (RMMF).

Author Contributions

M.T., S.W., S.S., and M.B. conceived the project. M.T. undertook thin film synthesis and materials characterisation (with contributions from T.A.). All aforementioned authors analysed and interpreted the data. D.H. and W.W. designed terahertz characterisation experiments, undertook measurements, and performed data analysis. M.T. and S.W. wrote the first draft of the manuscript with all authors contributing to the final document.

Additional Information

Supplementary information accompanies this paper at <https://doi.org/10.1038/s41598-017-17937-3>.

Competing Interests: The authors declare that they have no competing interests.

Publisher's note: Springer Nature remains neutral with regard to jurisdictional claims in published maps and institutional affiliations.



Open Access This article is licensed under a Creative Commons Attribution 4.0 International License, which permits use, sharing, adaptation, distribution and reproduction in any medium or format, as long as you give appropriate credit to the original author(s) and the source, provide a link to the Creative Commons license, and indicate if changes were made. The images or other third party material in this article are included in the article's Creative Commons license, unless indicated otherwise in a credit line to the material. If material is not included in the article's Creative Commons license and your intended use is not permitted by statutory regulation or exceeds the permitted use, you will need to obtain permission directly from the copyright holder. To view a copy of this license, visit <http://creativecommons.org/licenses/by/4.0/>.

© The Author(s) 2017